

DETERMINING DEPTH FROM REMOTELY-SENSED IMAGES

Robert A. Dalrymple, F. ASCE, Andrew B. Kennedy,
James T. Kirby, M. ASCE, and Qin Chen, M. ASCE¹

Abstract *Remotely-sensed images can provide synoptic or nearly synoptic data for large areas of the sea surface. Photographic and, more recently, radar measurement techniques can resolve the pattern of waves on the water surface and can provide a very dense sampling of kinematical variables of interest, ranging from a complete picture of the wave phase (in the case of single photographs) to horizontal velocity components at the water surface resulting from wind, tides, or waves (in the case of advanced radar techniques). When applied in the coastal zone, these images contain surface waves that are propagating over a complex bottom bathymetry and current field, and that are affected by a combination of shoaling, refraction, diffraction and nonlinear processes. This paper examines two methods to determine bathymetry from surface elevation information. The first is to examine the ability of linear dispersion relationship models to determine bathymetry, in cases with refraction and diffraction, and the second, based on lagged correlation method (and several images), is more generally useful for application.*

Introduction

Remote sensing of the ocean surface can provide a great deal of information about the sea. Since World War II, it has been desirable to make use of images of the sea surface to deduce the bathymetry and nearshore current structure of a region of interest. The advantages of remote sensing systems for bathymetric and current surveys are that they can be more rapid than ground based methods, the cost per survey is lower, and it is less hazardous (in terms of exposure to the elements or hostile activity).

There are a variety of possible remote sensing systems. Satellites now provide wind speed and wave heights by altimetry. Aircraft with radars: synthetic aperture radar (SAR) and interferometric SAR (INSAR) provide the ability to measure waves and currents. Some bathymetric data is being gleaned from the modulation of currents by the bottom from SAR data now, such as the ARGOSS BAS system in the Netherlands. LIDAR, using lasers from helicopters, such as the U.S. Army Corps of Engineers' SHOALS system (Lillycrop, Parson, and Irish, 1996), can provide bathymetric information at a rate of 5 km² per hour, with accuracies of ± 3 m horizontally

¹all at the Center for Applied Coastal Research, University of Delaware, Newark, DE 19716 USA

and ± 15 cm vertically in water depths of 40 m or less—provided that the water is reasonably clear. Turbidity affects the depths to which this methodology can be used.

An image of the water surface will contain information about the wave length of the surface waves, $L(x, y)$, which may vary with position, denoted by the horizontal coordinates x and y . Methods based on simple approaches (such as using the linear wave dispersion relationship to estimate local water depth from local estimates of wave length and period) provide an initial indication of the variation of depth in intermediate water depths, where nonlinearity is weak and currents typically are not the leading order factor in determining wave properties. The usual linear wave theory dispersion relationship is $\sigma^2 = gk \tanh kh$, where the wave angular frequency $\sigma = 2\pi/T$, where T is the wave period and the wave number k is $2\pi/L$. The wave period, assumed to be constant over the image, is determined from assuming a deep water wave length in a portion of the image or some other means.

Rearranging the dispersion relationship,

$$h(x, y) = \frac{1}{k(x, y)} \tanh^{-1}(\sigma^2/g)$$

Gleaning the wave length, $L(x, y)$, from an image, however, is not without error. There may be errors in the measurement technique and there may also be errors in how the wave period is determined.

Taking the derivative of the above equation and then dividing by $h(x, y)$, we have the relative error in depth as a function of the relative error in the wave angular frequency and the wave number.

$$\left(\frac{dh}{h}\right) = 2 \left(\frac{\sinh 2kh}{2kh}\right) \left(\frac{d\sigma}{\sigma}\right) - \left(1 + \frac{\sinh 2kh}{2kh}\right) \left(\frac{dk}{k}\right) = f(kh) \left(\frac{d\sigma}{\sigma}\right) - g(kh) \left(\frac{dk}{k}\right), \quad (1)$$

which defines two functions, $f(kh)$ and $g(kh)$, which determine the relative contributions of the percentage errors in angular frequency and wave number to the percentage error in the depth. These error terms are equal to two in shallow water, meaning that any errors in wave length determination are multiplied by this factor of two. What is worse is that these terms grow exponentially with kh . (Errors in wave length lead to the same size errors in wave number, as $dk/k = -dL/L$.) Figure 1 shows how $f(kh)$ and $g(kh)$ grow with depth. Clearly, the relative depth becomes far more sensitive to error as the depth increases.

Close to shore, nonlinearity can become a dominating factor in determining wave properties. Further, since waves are rapidly evolving and do not correspond well to any particular permanent form solution, it is likely to be difficult to parameterise nonlinear effects in a useful form. (Grilli and Skourup (1998, this proceedings) have examined the depth inversion of nonlinear periodic waves using a fully nonlinear boundary element method.)

This paper reports on bathymetry determination from "remotely sensed" (actually synthetically generated) images using two different methods. First, we determine the ability of the linear wave theory to determine the bathymetry from water surface elevations obtained by wave models over given bathymetry. Then we utilize a maximum

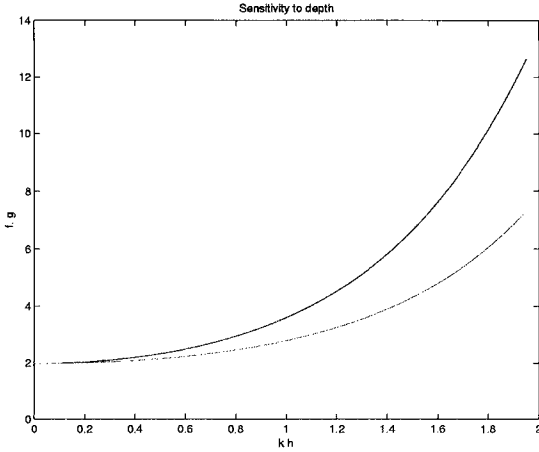


Figure 1: Plot of $f(kh)$ and $g(kh)$ versus kh . Upper line is $g(kh)$.

entropy method with a time series of synthetic images taken over a short period of time (comparable to a wave period).

Hilbert Transform

REF/DIF 1 is a forward scattering parabolic wave model (Kirby and Dalrymple, 1983, 1984, 1992) that predicts refraction and diffraction. This model was run with a simple idealized geometry (the Berkhoff, Booij, and Radder (1982) basin test, denoted BBR, which includes oblique wave incidence on a 1:50 planar beach with an elliptical shoal), using the BBR wave conditions, and surface elevations were computed by the model on a 200 by 200 grid (each grid is 0.125m x 0.125 m). These surface elevations (which have been shown to agree with measurements extremely well) were then used as the "remotely sensed" data and analysed for bathymetry.

To obtain the phase of the waves within the "image," a Hilbert transform was used along the 200 onshore grid lines. The Hilbert transform converts real time series into complex series from which the phase may be obtained. [In Matlab, this involves three steps: `unwrap(phase(hilbert(data)))`]. The `unwrap` command ensures that the phase increases monotonically, instead of staying in the range $-\pi$ to π . The horizontal gradient of the phase over the image then provides the local wave numbers, from which the depths are determined using the linear theory dispersion relationship and the given wave period ($T=1$ s).

Figure 2 shows the results for the BBR data set. Note that the depth inversion (using a linear dispersion relationship in **REF/DIF 1**) gives quite good results except in the focussing/diffraction region behind the shoal, where very sharp ridges of unreal channels and bars occur. This is due to the fact that the wave length determination

is difficult where waves are short-crested and diffraction is strong.

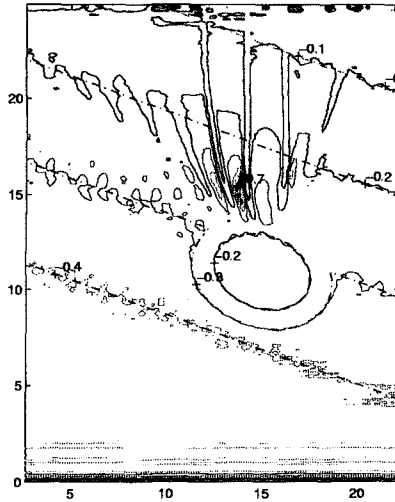


Figure 2: Depth inversion of **REF/DIF 1** output for BBR data set, showing the actual bathymetry (dashed lines) and the determined bathymetry (solid lines).

Applying a 2-D Fourier smoothing algorithm to the determined depths removes the sharp changes in depth produced by the focussing, as shown in Figure 3. (Note that we do introduce boundary effects due to the assumed spatial periodicity required by the Fourier filtering.) However, in the middle of the figure, the shoal is clearly and accurately picked out by the depth-inversion algorithm.

No remotely-sensed image will be as free of noise as model output. Variations in the field data will occur due to spectral sea effects, wind, capillary waves, specular reflections, etc. Therefore we introduced random noise to model output to determine the effect on the inversion algorithm. Figure 5 shows the bathymetry deduced by surface elevation data which have a 10% normally distributed random variation added. While the results are not as good as the no-noise case, the depths are reasonably well delineated. More noise results in seriously degraded bathymetry.

Additional examinations of the method included determining the errors involved with increasing the random noise and using the incorrect wave period. Further these comparisons were carried out with data from the linear **REF/DIF 1** run along with a nonlinear model computation (using a composite dispersion relationship that fits the deep water Stokes relationship to a shallow water form). The variation of error introduced by these noise and period effects are shown in Figures 7 and 8.

While comparisons of linear and nonlinear versions of **REF/DIF** to the laboratory data show important differences, the bathymetry obtained from linear and nonlinear

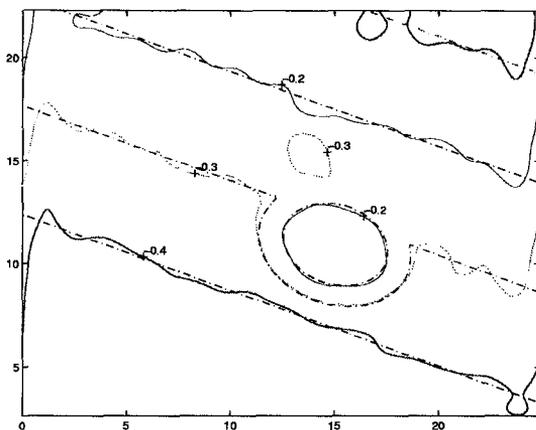


Figure 3: 2-D smoothed depth inversion of **REF/DIF 1** output for BBR data set, showing the actual bathymetry (dashed lines) and the smoothed bathymetry (solid lines).

synthesized surface data using the linear dispersion relationship for both cases show no real differences over the shoal and that the shoal is accurately found, even in the presence of noise introduced into the surface wave image. This method is extremely sensitive to the wave period, however.

All tests here have been done with a single frequency incident wave. A spectral sea state is best treated by the next method, which requires a sequence of images in time to determine wave frequencies.

Lag-Correlation Methods

Sequential images of a water surface taken at reasonably short time intervals show waves of varying directions and wave numbers propagating through space at their characteristic phase speeds. This is the basis of the lag-correlation methods, where the sequential images are used to determine a relationship between wave number and frequency, and thus to estimate depth. For large spatial records where the wave number spectrum is constant over the image and sequential images are available, wave number spectra and the associated phase speeds may be easily determined using standard Fourier techniques. However, in coastal regions, wave lengths and directions may change significantly over several wave lengths, making direct methods like this impossible. In this case, different methods must be used to estimate the wave number spectrum and associated phase speeds. Note that here the spectrum is characterised

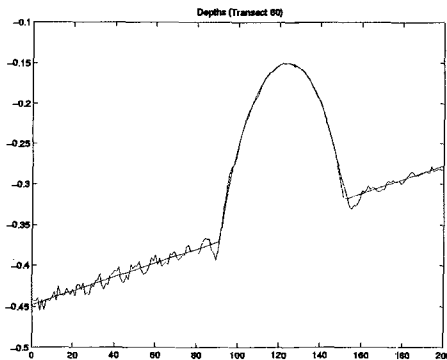


Figure 4: 2-D smoothed depth inversion of **REF/DIF 1** output for BBR data set, along on/offshore transect 80, showing the actual bathymetry and the inferred bathymetry (wavy line).

in terms of wave number rather than frequency, which is much more natural given the form of the data. The methods used here will make the assumption that the wave field is approximately stationary over a window of about two peak wave lengths. Although this assumption becomes invalid near the shore, and in areas with strong changes in bottom topography, it remains reasonable for many situations.

To aid analysis, the surface elevation data contained in the windows of interest is transformed into auto and cross correlation functions (e.g. Bendat and Piersol, 1986, Balakrishnan, 1995). Auto correlation functions of some window of data show the correlation of an image with itself at different spatial lags. If sequential images of the same window are compared, a cross-correlation function results. Autocorrelation functions contain information about the wave number spectrum to within a 180 degree directional ambiguity, while the addition of cross-correlation functions resolves this ambiguity and provides information about phase speed. Auto and cross correlation functions may also be easily constructed from a given wave number spectrum and dispersion relationship. For full and accurate records of auto and cross correlation functions, the wave number spectrum and dispersion relationship may be easily found, and the depth may be deduced from this. However, window sizes are assumed to be only about two peak wave lengths, and because of way they were constructed from data, correlation functions with high lags become unreliable. Therefore, since full records are unavailable, more approximate methods must be used to find the wave number spectrum and, more importantly, the dispersion relationship and therefore the depth.

One Horizontal Dimension

As a first test, the lag-correlation method was tested for one horizontal dimension. Spatial images of the water surface were generated using a fully nonlinear extended

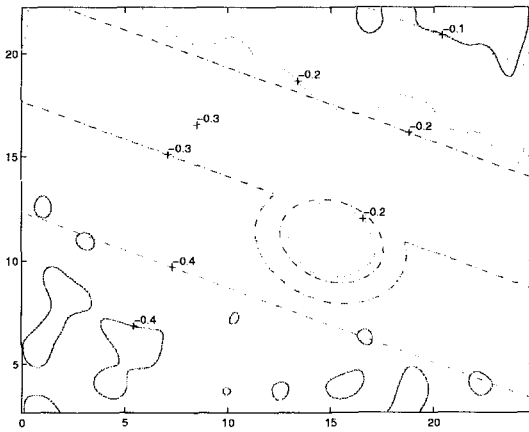


Figure 5: 2-D Smoothed Depth inversion of **REF/DIF 1** output for BBR data set, showing the actual bathymetry (dashed lines) and the smoothed bathymetry (solid lines).

Boussinesq model (Wei et al., 1995) over a bar-trough topography (Figure 9). The surface was then divided into overlapping windows with a length of about two peak wave lengths. Unbiased auto and cross correlations, which include a factor to correct for finite record length, were then computed in these windows. Ten sequential images were used to provide data; multiple auto and cross correlations were thus averaged to reduce error. However, there remained significant error for high spatial lags, and all correlations for lags greater than $2/3$ of the window size were considered unreliable and discarded.

The inverse problem was then solved on a window by window basis. In each window, the measured auto and cross correlations were assumed to come from a spectrum that had either a JONSWAP or TMA type form (results were almost identical for both). The unit spectrum of this form was defined by a peak wave number, k_p , and a peak enhancement factor, γ . In order to specify the dispersion relationship for calculating cross correlations, a depth h also needed to be specified. Initially, of course, none of these were known, although a reasonable estimate could be made for the peak wave number. Initial guesses were made for each which were then iterated until the squared error between the measured and estimated auto and cross correlations was at a minimum. The depth at this minimum was then assumed to be the inversion depth.

Figure 9 shows actual and estimated depths for an incident spectrum with peak $T_p = 7s$ and height $H_{RMS} = 0.025m$. The time lag between sequential images was 2s. Agreement is quite good, although small scale features cannot be reproduced.

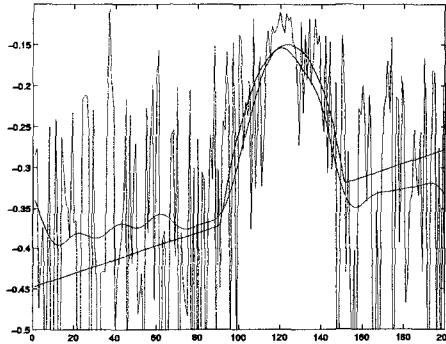


Figure 6: 2-D smoothed depth inversion of REF/DIF 1 output for BBR data set, along transect 80, showing the actual bathymetry, the inferred bathymetry (no smoothing (very wavy line)), and the smoothed bathymetry.

Furthermore, some scatter is clearly visible. This is likely due to a finite record length, and the resulting error in the correlation functions. Errors are greatest for deeper depths because here, the dependence of phase speed on depth is small. Thus, small errors in estimating phase speed or wave number will be magnified.

Figures 10-11 show inversions performed over the same topography as RMS wave heights increase. The time series of input waves to the Boussinesq model remained identical except for a multiplicative factor. Nonlinearities would, of course become evident as waves evolved. The main effect of this nonlinearity is to overestimate water depth wherever wave heights are large. This is because of amplitude dispersion, which increases with phase speed. Evidently, as shown by Grilli and Skourup (1998), using a nonlinear celerity would increase accuracy.

Two Horizontal Dimensions

For two horizontal dimensions the general problem remains the same: find a wave number spectrum and associated depth to best match the measured auto and cross correlation functions. However, it is more difficult to define a two dimensional wave number spectrum in terms of a few parameters - particularly if the spectrum has more than one dominant wave number or direction.

Accordingly, a more general technique was used to estimate the wave number spectrum in each window. The maximum entropy technique of Lim and Malik (1981) has been shown to be useful for finding the maximum entropy spectrum for two dimensional wave number problems from incomplete autocorrelation data. This technique uses two dimensional FFT's to transform between autocorrelation and wave number space, and again between wave number space and constraint space until a maximum entropy spectrum is reached that satisfies the measured constraints on the autocorrelation function. A variant of this method was used to compute the wave number

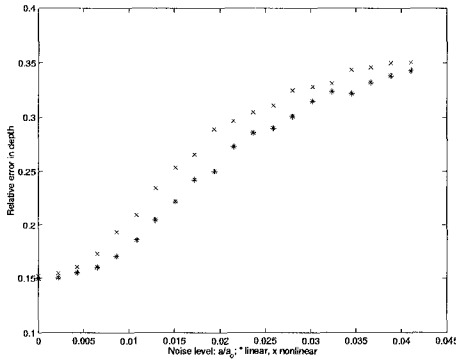


Figure 7: Relative errors introduced by uniform random noise for linear and nonlinear REF/DIF results.

spectrum directly from the autocorrelation function. In some cases, the method may be slow to completely converge, but it was found that complete convergence was not necessary to accurately invert depths. As long as the peak of the wave number spectrum was in the correct location, results continued to be accurate.

Once the wave number spectrum had been computed, the depth in each window was iterated until the cross correlation function resulting from the maximum entropy spectrum best matched the measured function. A 180 degree ambiguity with respect to the wave number spectrum had to be specified, but this was a minor concern. Figure 12 shows estimated and actual depths for the Berkhoff, Booij and Radder (1982) experiment described earlier. Once again, agreement is quite good, although the depth at the top of the shoal is overestimated, due to nonlinearities and/or a finite window size. Figure 13 gives a one dimensional slice through the shoal, and clearly shows the overprediction of depth on top of the shoal. This is almost certainly because depth is assumed to be constant throughout the analysis windows, an assumption that is violated in the region of the shoal.

Next, to test the effect of inaccuracies in the measurements, Gaussian noise with a standard deviation of 10 percent of the wave height was added to the data. Depths were then estimated as before. Figure 14 shows the computed and measured depths. These are virtually identical to those computed earlier. This insensitivity is because the maximum entropy technique transforms white noise in the data into a noise floor in the wave number spectrum. This noise has no strong correlation with depth and thus does not affect greatly estimates of depth. Figure 15 shows a slice through the shoal and again the results are almost identical to the no noise case.

Appendix: References

Alpers, W., and Hennings, I., "A Theory of the imaging of underwater bottom topography by real and synthetic aperture radar," *Journal of Geophysical Research*,

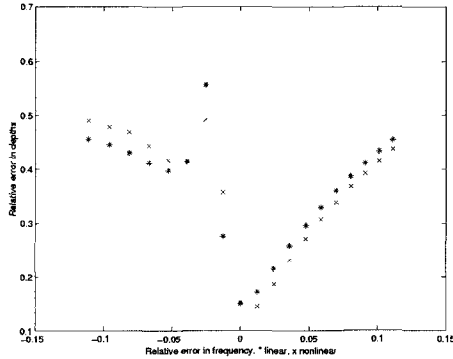


Figure 8: Relative errors introduced by relative errors in angular frequency for linear and nonlinear REF/DIF results.

89, C6, 10,529-10,546, November 20, 1984.

Balakrishnan, A.V., 1995, "Introduction to random processes in engineering", Wiley-Interscience, New York.

Bendat, J.C. and Piersol, A.G., "Random data: analysis and measurement procedures", Wiley-Interscience, New York, 1986.

Berkhoff, J.C.W., N. Booij, and A.C. Radder, "Verification of numerical wave propagation models for simple harmonic linear water waves," *Coastal Engrg.*, 6, 255-279, 1982.

Grilli, S.T. and Skourup, J., "Depth inversion in shallow water based on properties of nonlinear shoaling waves", *Proc. 26th Int. Conf. Coastal Eng.*, Copenhagen, 1998.

Kirby, J.T. and R.A. Dalrymple, "A Parabolic Equation for the Combined Refraction-Diffraction of Stokes Waves by Mildly Varying Topography," *J. Fluid Mechanics*, 136, 453-466, 1983.

Kirby, J.T. and R.A. Dalrymple, "Verification of a parabolic equation for propagation of weakly-nonlinear waves," *Coastal Engrg.*, 9, 219-232, 1984.

Kirby, J.T. and R.A. Dalrymple, "Combined Refraction/Diffraction Model-REF/DIF 1, Version 2.5," Center for Applied Coastal Research, Res. Rpt. CACR-94-22, 1994.

Lillicrop, W.J., L.E. Parson, and J.L. Irish, "Development and Operation of the SHOALS Airborne Lidar Hydrographic Survey System," *SPIE Laser Remote Sensing of Natural Waters: From Theory to Practice*, 2964, 26-37, 1996

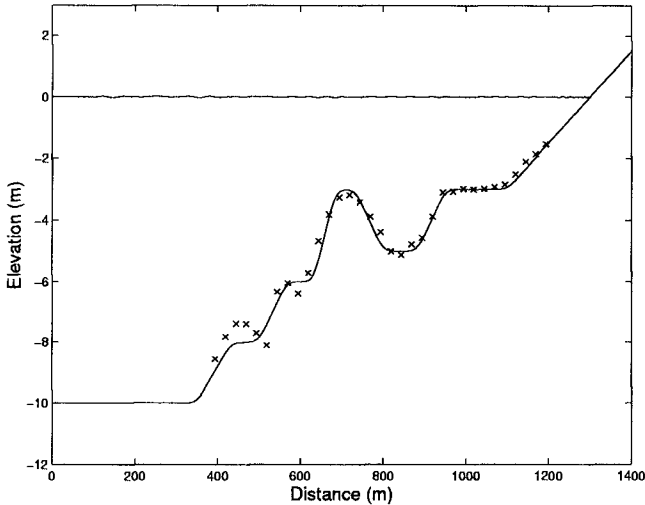


Figure 9: Estimated (\times) and actual (-) depths over a bar-trough topography, $H_{RMS} = 0.025$ m

- Lim, J.S. and Malik, N.A., 1981, "A new algorithm for two-dimensional maximum entropy power spectrum estimation", *IEEE Trans. Acoust., Speech, Signal Processing*, **29**, 401-413.
- Schuchman, R.A., Lyzenga, D.R., and G.A. Meadows, "Synthetic aperture radar imaging of ocean-bottom topography via tidal current interactions: Theory and observations", *Int. J. of Remote Sensing*, **6**, 1179-1200, 1985.
- Wei, G., Kirby, J. T., Grilli, S. T. and Subramanya, R., 1995, "A fully nonlinear Boussinesq model for surface waves. I. Highly nonlinear, unsteady waves", *Journal of Fluid Mechanics*, **294**, 71-92.

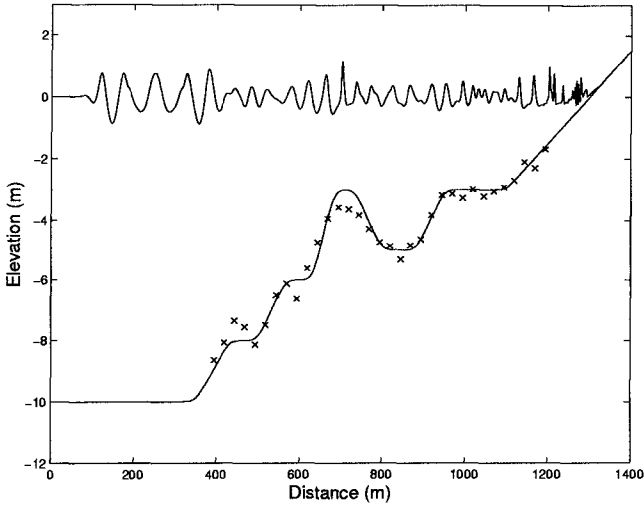


Figure 10: Estimated (x) and actual (-) depths over a bar-trough topography, $H_{RMS} = 1$ m

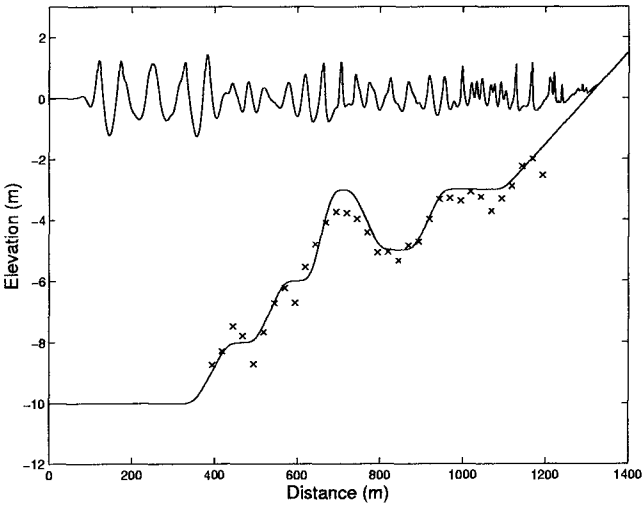


Figure 11: Estimated (x) and actual (-) depths over a bar-trough topography, $H_{RMS} = 1.5$ m

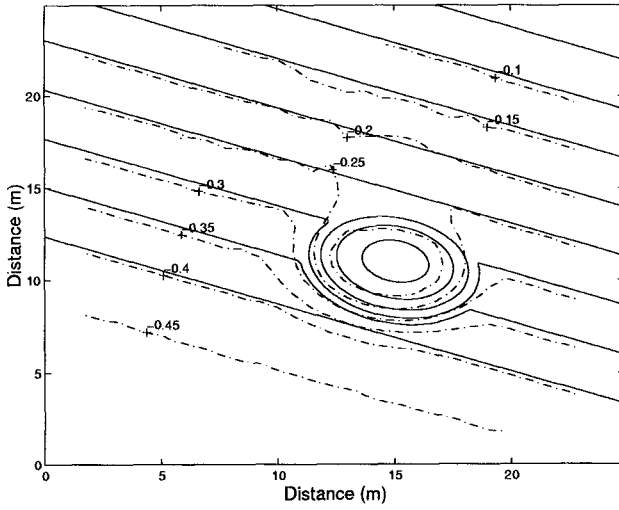


Figure 12: Depth contours over the BBR shoal (-) actual; (- - -) estimated

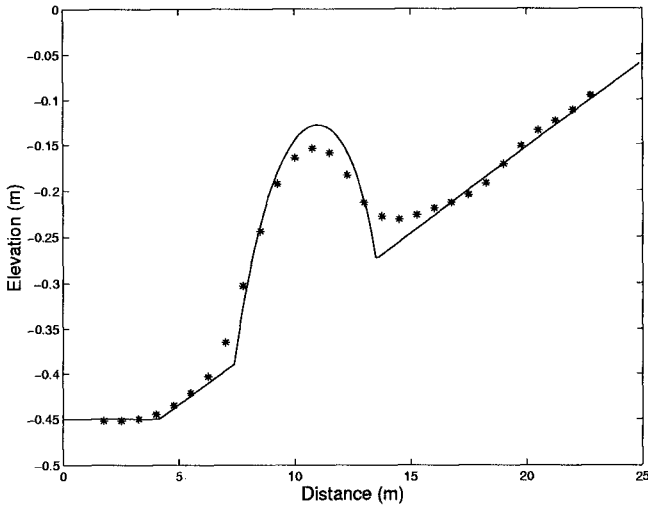


Figure 13: Cross section of depth through the BBR shoal, (-) actual; (*) estimated

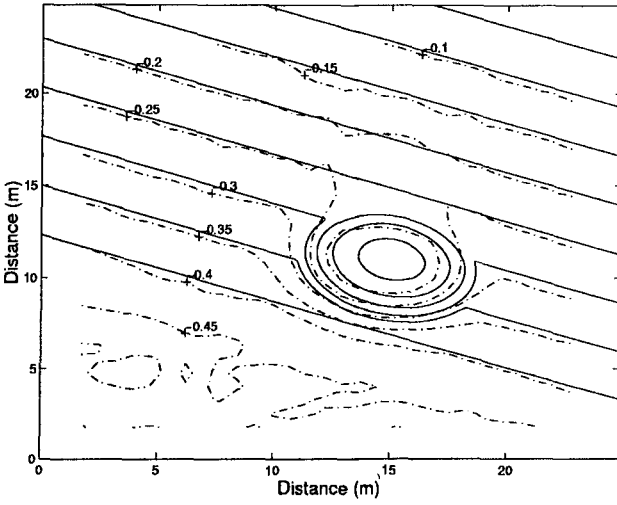


Figure 14: Depth contours over the BBR shoal (-) actual; (- - -) estimated from noisy data

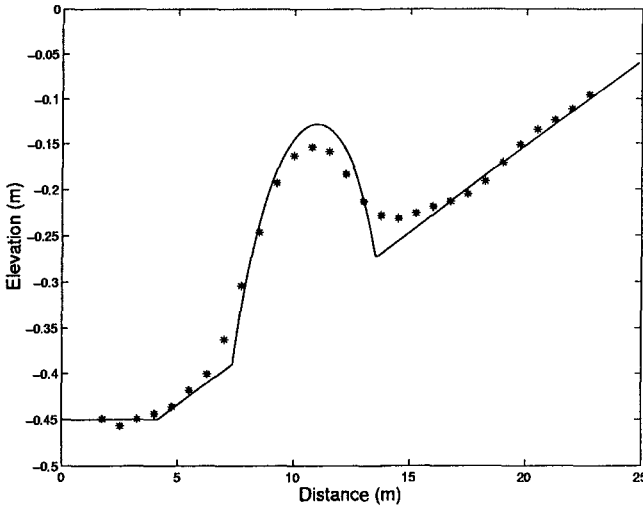


Figure 15: Cross section of depth through the BBR shoal, (-) actual; (*) estimated from noisy data